Cleaner Engineering and Technology 11 (2022) 100562

Contents lists available at ScienceDirect

Cleaner Engineering and Technology

journal homepage: www.sciencedirect.com/journal/cleaner-engineering-and-technology

Small-scale energy potential from salinity gradients at a transboundary riverine estuary in the Yucatán Peninsula

Juan Carlos Alcérreca-Huerta [a,*], Mariana Elvira Callejas-Jiménez [b], Laura Carrillo [b]

[a] Consejo Nacional de Ciencia y Tecnología-El Colegio de la Frontera Sur (CONACYT-ECOSUR), Department of Observation and Study of the Land, the Atmosphere and the Ocean, Av. del Centenario km 5.5, Chetumal, Mexico
[b] El Colegio de la Frontera Sur, Department of Observation and Study of the Land, the Atmosphere and the Ocean, Av. del Centenario km 5.5, Chetumal, Mexico

ARTICLE INFO

Keywords:
Salinity gradient energy
Gibbs free energy
Marine energy
Yucatán peninsula
Mexico–Belize riverine Estuary

ABSTRACT

This study estimates the environmental and technical energy potential of the thermohaline conditions in the Mexico–Belize riverine estuary. Site-specific conditions were considered based on monthly water temperature, salinity, and river discharge field measurements along the Hondo River estuary from 2018 to 2019. The practical extractable energy assessment described the possibility of outlining a hypothetical ~3 MW salinity gradient energy (SGE) plant, which could support 5.4–15.1% of houses in the main urbanised area. Low-income housing benefits can be viable for up to 7700 houses with either mechanical or natural ventilation under tropical weather conditions. Alternatively, this energy may be directed towards commercial shared zones between Mexico and Belize. SGE harnessing might be possible throughout the year with limited zero extraction periods provided by seasonal thermohaline variations in the estuary during the dry season and at mid-summer droughts. The energy potential of the Hondo River was compared with manatee presence to explore possible environmental implications from SGE harnessing. The periods of high energy potential were followed by peaks in manatee sightings with a 1–2-month delay. The SGE approach based on a small-scale energy-generation scheme for the local coastal urbanised area considering the binational framework is discussed.

1. Introduction

Reliable, efficient, and affordable access to energy enhances human livelihoods (Pachauri et al., 2012). On behalf of this, alternative renewable energy sources are explored to contribute and diversify the energy matrix. Additionally, local generation sources can reinforce the effectiveness of central grids (Deshmukh et al., 2013). Small-scale energy-generation schemes have been more effective in producing these benefits, although large-scale programmes are more financially viable (Burton and Hubacek, 2007). Natural resource extraction and energy generation under small-scale schemes decrease the intervened spaces and the extent of their impact while discouraging oppositional reactions that could trigger conflicts (Kauffer, 2021).

Salinity gradient energy (SGE) can support part of the increasing energy demands despite being in the early stages of development (Seyfried et al., 2019), with a global SGE potential between 1650–2000 TWh/yr (Budde, 2021). Consequently, estuaries and river mouths are considered potential renewable energy sources because of the entropy of mixing of water at different salt concentrations (Khodadadian Elikaiy et al., 2021), which depends on intrusion length and flushing times (Haddout and Priya, 2020). Therefore, SGE involves natural temporal and spatial variations that modify the salinity and reduce the theoretical potential (Alvarez-Silva et al., 2014). These variations promote the functionality and environmental differentiation of river estuarine habitats.

Research based on field datasets or multiannual monitoring schemes of the thermohaline conditions of estuarine environments is limited when directed towards assessing the SGE potential (Marin-Coria et al., 2021). Contemporary research has alternatively focused on the local environmental impact of SGE (Seyfried et al., 2019); life cycle assessment (Mueller et al., 2021); modelling of estuarine hydrodynamics coupled with energy production models (Zachopoulos et al., 2022); and multidisciplinary approaches for SGE on-site potential considering technical, technological and market analysis (Roldan-Carvajal et al., 2021) or socioecological features (Wojtarowski et al., 2021). However, specific site analyses and *in-situ* field measurements of estuarine physical features are required for current SGE research approaches.

Pilot programmes and the exploration of site-specific SGE plants are

* Corresponding author.
E-mail address: jalcerrecah@ecosur.mx (J.C. Alcérreca-Huerta).

https://doi.org/10.1016/j.clet.2022.100562
Received 19 April 2022; Received in revised form 12 September 2022; Accepted 25 September 2022
Available online 28 September 2022

scarce and mainly developed for testing facility technologies. For instance, prototype 1, 10, 50 kW systems have been installed in Trapani, Italy (Tedesco et al., 2017); in Tofte, Norway (Kempener and Neumann, 2014); as well as Breezanddijk (Yip et al., 2016) and Affsuitdijk (Schaetzle and Buisman, 2015) in the Netherlands, respectively. Theoretical and practical energy potentials in large-scale schemes have been assessed to demonstrate the SGE harnessing feasibility. SGE potential feasibility with an energy supply capacity of 10°–10^{1} GW is studied from either pairing river water and hypersaline water lagoon systems, such as Lake Van, Turkey; Lake Eyre, Australia; and Lake Urmia, Iran (Helfer et al., 2013), or freshwater and seawater at river mouths (Alvarez-Silva and Osorio, 2015). Nevertheless, small-scale schemes and considerations of site-specific constraints and opportunities suitable to meet the local energy supply have rarely been analysed. Moreover, approximately 23% of the international borders are defined by rivers (Popelka and Smith, 2020), which converge into estuaries that demand integrated transnational resource management strategies.

Therefore, this study assesses the Mexico- Belize riverine estuary's environmental and theoretical SGE potential to identify feasible scenarios for local energy supply. The energy yield assessment considered site-specific conditions based on the temporal variability of the thermohaline structure in the riverine estuary. For this purpose, monthly field measurements were conducted from 2018 to 2019. The possibility is shown for outlining a hypothetical SGE plant, which could potentially address local energy consumption in Mexico and Belize. Furthermore, the practical SGE potential was compared with manatee presence to explore possible environmental implications of SGE harnessing. The benefits of local SGE implementation are briefly discussed for the planning, regulation, and environmental management of natural resources generally constrained by local political and legal territorial delimitations.

2. Methods

2.1. Study area

The study area is located along the natural border between Mexico and Belize, outlined by the Hondo River in the south-eastern portion of the Yucatán Peninsula (Fig. 1). The Hondo River estuary results from the mixture of freshwater from the river and brackish water of the binational Chetumal–Corozal Bay (Callejas-Jiménez et al., 2021), where microtidal conditions develop with amplitudes <0.10 m, and the estuarine hydrodynamics are mainly controlled by wind and runoff episodes (Carrillo et al., 2009b) (Fig. 1). The riverine estuary varies in width, ranging from 60 to 130 m before reaching its funnel-shaped delta. Moreover, estuarine conditions reportedly extend over the river course about 7–20 km from the river mouth. The riverine estuary and the bay present mesohaline conditions since the marine influence in the area is limited (Carrillo et al., 2009b).

Typical tropical seasonality in the study area (Carrillo et al., 2009a) the Hondo River estuary hydrodynamics (Callejas-Jiménez et al., 2021). The rainy season (RaS) features variable rainfall and runoff episodes due to trade winds, storms, and hurricanes between May and October. A dry season (DrS) occurs between February and April, with low precipitation rates and increased temperatures. The regionally known *Nortes* season (NoS) is defined by cold fronts, moderate rainfall, and intense northerly winds between October and February. Particularly between July and August, a mid-summer drought occurs in the study area due to high-pressure systems constraining cloud formation, thereby increasing solar radiation and reducing precipitation rates (Corrales-Suastegui et al., 2020).

Population settlements are located along the riverine estuary and river mouth, with Chetumal City as the largest urbanised area with approximately 169,000 inhabitants (Fig. 1) (INEGI, 2021). The locality of the Corozal Free Zone (CFZ) in Belize over the river estuary promotes trade, manufacturing, and import/export services with an annual revenue value of 400 million USD (CBB, 2019). Foreign trade electricity interconnections between Mexico and Belize with 50 MW capacity and lines with 115-kV tension under a permanent interconnection framework currently exist in the study area. As a result, the international border relationship along the Hondo River estuary is defined by cross-border trades, transboundary checkpoints, urban-use policies, tourism, and binational commercial growth primarily based on the natural resources of the area (Vivid Economics, 2019).

2.2. Field measurements, sampling techniques, and preliminary data analysis

Measurements were conducted monthly in 2018 and 2019 along an approximately 28 km long transect of the Hondo River estuary to

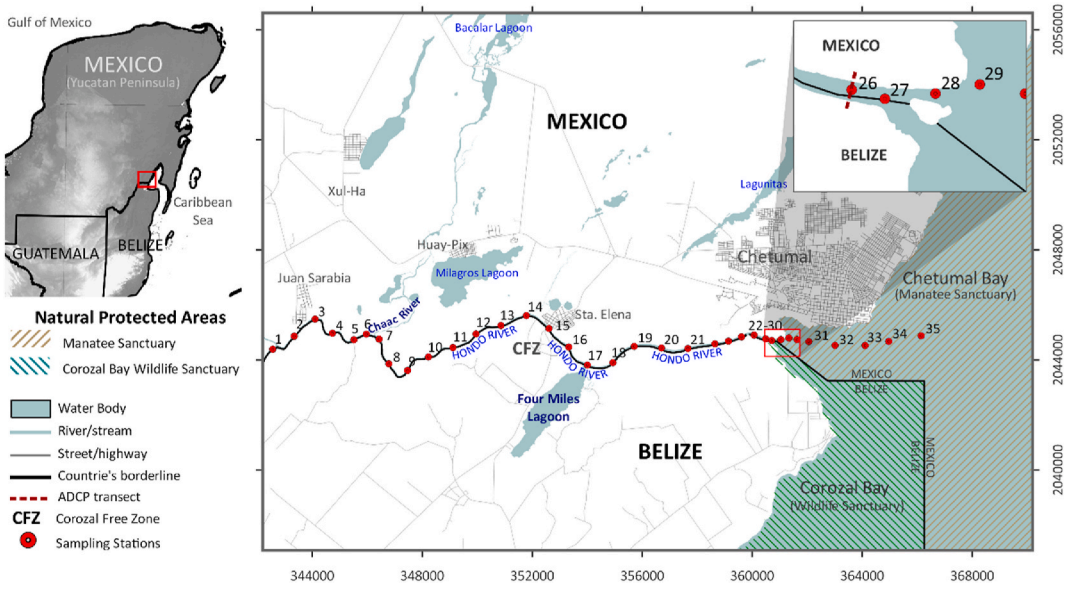

Fig. 1. Riverine estuary environment of the Hondo River over the international border of Mexico and Belize (UTM 16N). Population settlements, natural protected areas, and surrounding water bodies in the study area for Mexico (INEGI, 2022) and Belize (Meerman and Clabaugh, 2017) are shown together with the location of sampling stations and ADCP transects for monthly measurements.

account for the spatio-temporal variations in the thermohaline gradients. Approximately 35 sampling stations (St.) were defined in the study area and organized as follows: 28 in the river estuary (St. 1–28), 5 in the river delta (St. 29–33), and 2 in the Chetumal Bay (St. 34–35) (Fig. 1). A uniform spacing of 1 km was established between each station from St. 1 to St. 24 whereas a uniform spacing of 500 m was set for St. 25–28, and a uniform spacing of 250 m was set for St. 29–31. The station distances decreased according to the expected variations in the thermohaline gradients close to the river mouth. The spacing between stations again increased to 1 km after St. 31.

Water temperature, salinity, and density profiles were measured using a YSI CastAway®-CTD instrument at each sampling station. A Humminbird 899cxi HD SI sonar unit with a 200/83 kHz DualBeam PLUS^{TM} sonar system and integrated GPS was used to record longitudinal bathymetric data of the riverine estuary.

Monthly pycnoclines were estimated based on the locations of the highest vertical density gradients ($\partial\rho/\partial z$) from the density profiles of each station. Average salinity (S) and water temperature (T) profiles along the river estuary were calculated considering the two-year measurements. Similarly, the calculated monthly density profiles were averaged to estimate the mean pycnocline location for 2018–2019. The river profiles are described considering the longitudinal river distance (D_{RM}), being positive upstream of the river mouth located at 88.313461° W and 18.488753° N.

A stratification proxy was calculated using the surface-to-bottom differences in water temperature ($\Delta T_{BS} = T_{bottom}\text{-}T_{surface}$) and salinity ($\Delta S_{BS} = S_{bottom}\text{-}S_{surface}$). The maximum ΔT_{BS} and ΔS_{BS} values of each month were obtained to describe the maximum thermohaline differences ($\Delta T_{BS,\ max}$ and $\Delta S_{BS,\ max}$) at each location. Furthermore, the seasonality of the surface-to-bottom differences considered the mean value of ΔT_{BS} and ΔS_{BS} from the measurements between May and October for RaS; February and April for DrS; and October to February for NoS. The seasonal variations in surface-to-bottom differences are described as a function of the distance from the river mouth and later compared with the overall behaviour during the study period.

Velocity profiles were measured using a RiverPro Acoustic Doppler Current Profiler (ADCP) 1200 kHz RD Instruments from February 2018 to July 2019. The velocity profiles were measured at a cross-section of the Hondo River close to its mouth, at St. 26 prior to the river bifurcation by an island and the immediate flow into Chetumal–Corozal Bay (Fig. 1). Cross-sectional velocity measurements were repeated four times. The resulting velocity fields of each repetition were averaged and considered for analysis. Measurements were used to estimate the river discharge and detailed cross-sectional velocity fields related to the effects and variations in salt intrusion in the riverine estuary.

2.3. Theoretical energy potential and reliability analysis

Monthly temperature, salinity, and river discharge measurements were used to calculate the environmental and technical energy potential from the salinity gradients rather than to assume general averaged salinity and temperature values. Hence, the Gibbs free energy of mixing (ΔG_{mix}; J/m^3] resulting from mixing salt and freshwater was estimated considering the Gibbs free energy before (G_1) and after mixing (G_2) (Eq. (1)) (Emdadi et al., 2016):

$$\Delta G_{mix} = G_1 - G_2 = \left(G_s + G_f\right) - G_b \tag{1}$$

where G_1 is the sum of the free energy of the electrolytes in the mixing represented by salt (G_s) and freshwater (G_f), and G_2 is the free energy of the brackish water (G_b) solution after mixing. For ideal solutions, the Gibbs free energy (G_i) of each electrolyte (i = s, f, b) is a function of volume, salinity, temperature, and solution composition (Eq. (2)):

$$G_i = T_i m_i R[x_i \ln(x_i) + y_i \ln(y_i)] \tag{2}$$

where G_i is in W, T is the absolute temperature in K, m is the total moles per unit volume in mol/m^3, R is the universal gas constant (8.314 J/mol K), x is the molar fraction of ions, and y is the molar fraction of water. Generally, the contribution of water species is neglected compared to the contribution of ionic species. For strong electrolyte solutions, the contribution of multiple ionic species is introduced by ν. Hence, the Gibbs free energy is calculated as in Eq. (3) with $\nu = 2$ for NaCl (x_i) solutions since 1 mol of the salt dissociates into 2 mol of ionic species given by the cation-anion pair of Na^+ and Cl^- (Vallejo-Castaño and Sánchez-Sáenz, 2017).

$$G_i = T_i m_i R[x_i \ln (x_i)^{\nu}] \tag{3}$$

Once the Gibbs free energy of the estuarine water in its standard state within the Hondo River estuary (G_{HRE}) was assessed, it was introduced into a temperature-salinity (T–S) diagram to observe variations in energy, temperature, salinity, and density along the estuary. Sectional analyses of the G_{HRE} in river estuary were conducted considering its probability of occurrence at each kilometre.

The theoretical potential (TP) was calculated in terms of the Gibbs free energy and water flow rate Q in m^3/s (Eq. (4)) to assess feasible energy production from salinity gradients in W. The Gibbs energy for freshwater conditions (G_f) was calculated based on the depth-averaged salinity and water temperature at St. 1 (S_{RHo} and T_{RHo}). In contrast, salt conditions (G_S) were calculated based on the values at St. 35 (S_{BaCh} and T_{BaCh}). Eq. (5) was obtained by considering a 1:1 proportion of fresh and saltwater mixing to estimate TP so that $Q_B = Q_S + Q_f$, where Q_f is the net river discharge (Q_N) recorded from the ADCP transect at the river mouth (St. 26):

$$TP = \left(Q_s G_s + Q_f G_f\right) - Q_b G_b \tag{4}$$

$$TP = Q_N\left[\left(G_s + G_f\right) - 2G_b\right] \tag{5}$$

In addition, the practical extractable energy value (EE) to consider thermohaline gradients for electric energy conversion and human consumption depends on the TP, the extraction factor (EF), and the capacity factor (CF) as given in Eq. (6):

$$EE = EF \bullet TP \bullet CF \tag{6}$$

The EF is the design flow (Q_D) ratio to the mean river discharge (Q_{mean}). However, the design of an SGE plant should consider that the residual river flow (Q_R) after extraction (i.e. $Q_R = Q_{mean}\text{-}Q_D$) must not fall below the 'environmental flow' (Q_E), defined as the critical river discharge that avoids threatening the estuarine environment (i.e. $Q_R \geq Q_E$). This condition leads to different operational conditions (Alvarez-Silva et al., 2016): i) $Q_N > (Q_D + Q_E)$, full capacity operation; ii) $Q_E < Q_N < (Q_D + Q_E)$, partial capacity operation that leads to reduced extraction periods (REP); and iii) $Q_N < Q_E$, no operation resulting in zero extraction periods (ZEP). Considering the constraints of SGE plants given by EE and Q_E, the operational flow (Q_{OP}) is defined as $Q_{OP} = Q_D$ for full operation, $Q_{OP} = Q_N\text{-}Q_E$ during REP, and $Q_{OP} = 0$ for ZEP.

According to Alvarez-Silva et al. (2016), an EF of approximately 0.20 ($Q_D = 0.20\ Q_N$) and an environmental flow of $Q_E = 0.3Q_N$ reduce approximately 20% of the extraction periods, which might be suitable and reliable constraints for continuous SGE harnessing and environmental protection. Thus, to assess EE, EF = 0.20 and $Q_E = 0.3Q_N$ were assigned, respectively. The CF was calculated as the ratio of hours per year that the SGE plant operates with Q_{OP} to the ideal operation considering Q_D during the same time interval. The EE was ultimately expressed in full-load hours per year (Wh/yr) by multiplying the result in Eq. (6) by the total number of hours per year (8760 h/yr).

The environmental energy potential (EP) results from the relationship between TP and EF (Eq. (7)), which considered environmental constraints. EE and EP consider the average monthly TP calculated for the available measurements.

$$EP = EF \bullet TP \tag{7}$$

Finally, a possible contribution of SGE harvesting for local energy consumption was assessed using available information from low-income housing energy consumption under tropical weather conditions. The average theoretical energy potential was contrasted with the calculated percentage of manatee presence in the area based on Callejas-Jiménez et al. (2021) to identify possible effects of SGE extraction over this endangered species. For this purpose, the monthly sightings were graphically overlapped with the monthly energy potential behaviour.

3. Results

3.1. Thermohaline variations in the Hondo River estuary

Fig. 2 shows the average river water temperature and salinity profiles and the pycnoclines from monthly field measurements in 2018 and 2019. The pycnocline extended as far as $D_{RM}\approx22.6$ km upstream of the river mouth, where it reached a submerged mound (Fig. 2a). This coincided with a river change in orientation from a southwest-northeast direction to a west-east direction (Fig. 1). The maximum extent of the pycnocline occurred between June and December 2019. It was primarily associated with RaS (Fig. 3c). In contrast, the minimum extent of the pycnocline profile along the river occurred in March 2018, during DrS, with the development of a frontal zone close to the river mouth and toward Chetumal Bay between $D_{RM} \approx -2.3$ and $D_{RM} \approx -4.1$ km. Generally, the bottom frontal zone of the upper estuary is delimited by the pycnocline; however, it was shorter in 2018 than in 2019 (Fig. 2a), primarily during the NoS–DrS and DrS–RaS transitional periods. The average extent of the pycnocline profile is $D_{RM}\approx14.3$–16.1 km, where river mounds are developed, and water depths are reduced to d ≈ 4.0–6.5 m.

The average salinity profile described the development of a salt-wedge formation, extending approximately from $D_{RM}\approx14.3$–16.1 km to $D_{RM}\approx$ 22.6 km (Fig. 2b). Salinity values were, on average, S = 15.94 PSU at the limit of the river estuary with Chetumal Bay, decreasing upstream along the Hondo River estuary. Maximum and minimum salinities at St. 35 in Chetumal Bay were S = 24.88 PSU in September 2019 and S = 5.76 PSU in April 2019. Additionally, higher salinity values at St. 35 occurred during the RaS, whereas lower values occurred at the end of the NoS and during the DrS (i.e. between January and April).

The bottom-to-surface salinity difference (ΔS_{BS}) reached higher values during the RaS, decreased during the NoS, and continued decreasing during the DrS (Fig. 3a). The highest ΔS_{BS} for all seasons was $D_{RM}\approx2.0$–3.5 km, which coincided with a bathymetric depression of the river estuary with a water depth of d = 8.5 m. This depression was limited upstream by a mound of d = 5.0 m and downstream by the prominent river bottom ridge that forms the river delta, with the water depth changing from d = 8.5 m–2.0 m. Between $D_{RM}\approx$ 3.5 km and $D_{RM}\approx$ 14.3 km, the ΔS_{BS} presented a nearly constant value, depending on the season: $\Delta S_{BS}\approx13.3$ PSU for RaS, $\Delta S_{BS}\approx12.4$ PSU for NoS, and $\Delta S_{BS}\approx7.3$ PSU for DrS.

The value of ΔS_{BS} decreased continuously for $14.3<D_{RM}<22.6$ km, after which ΔS_{BS} was zero and only freshwater conditions were present. Similarly, for $D_{RM}<2.0$ km, the bottom-to-surface salinity difference was almost zero, describing a vertically mixed salinity condition at the river delta. The bottom-to-surface salinity difference increased from 2018 to 2019, with peaks during RaS (Fig. 3c). Moreover, the maximum bottom-to-surface salinity difference was $\Delta S_{BS,\ max}$ = 21.72 PSU in September 2019, which correlated with the maximum salinity in Chetumal Bay at

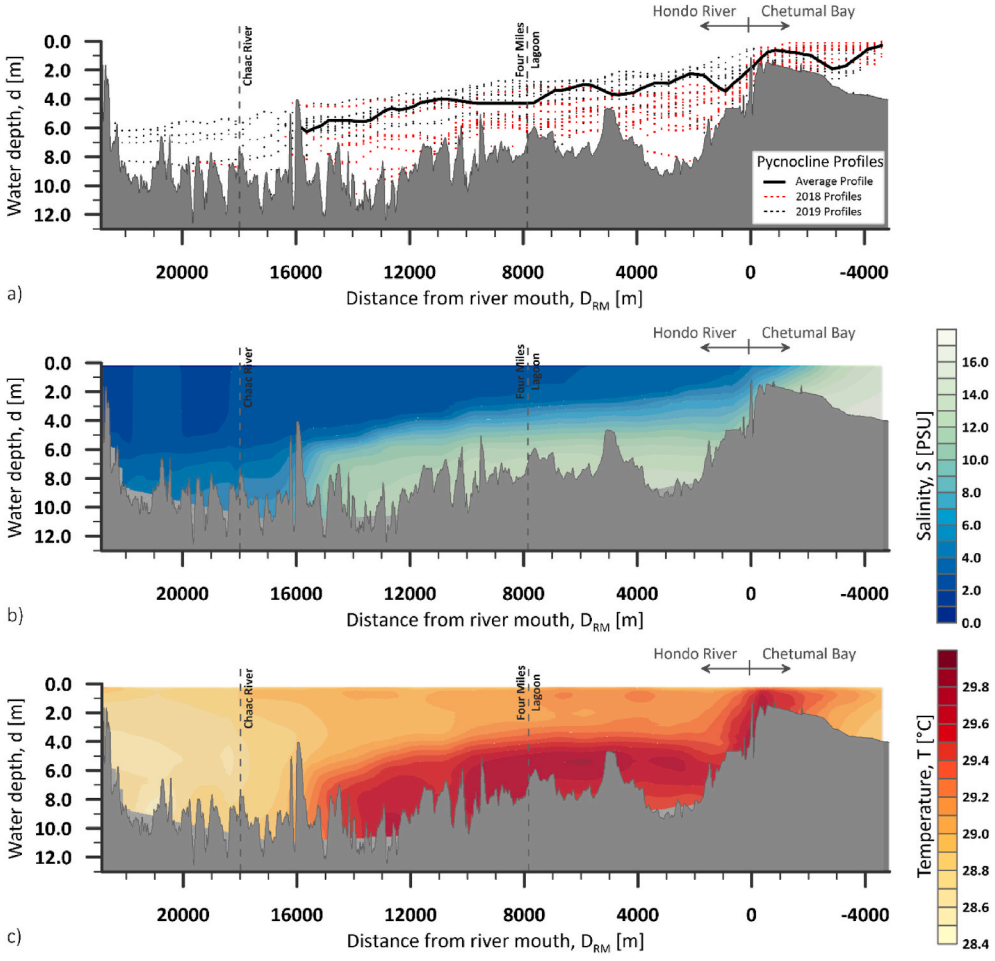

Fig. 2. Profiles of the riverine estuary with a) each pycnocline from field measurements during 2018 (red dots), 2019 (black dots), and the average pycnocline from the two-year measurements (black line), b) average salinity profile, and c) average temperature profile. Bathymetry of the Hondo River from field measurements is also depicted as a grey shaded area in the different panels. (For interpretation of the references to colour in this figure legend, the reader is referred to the Web version of this article.)

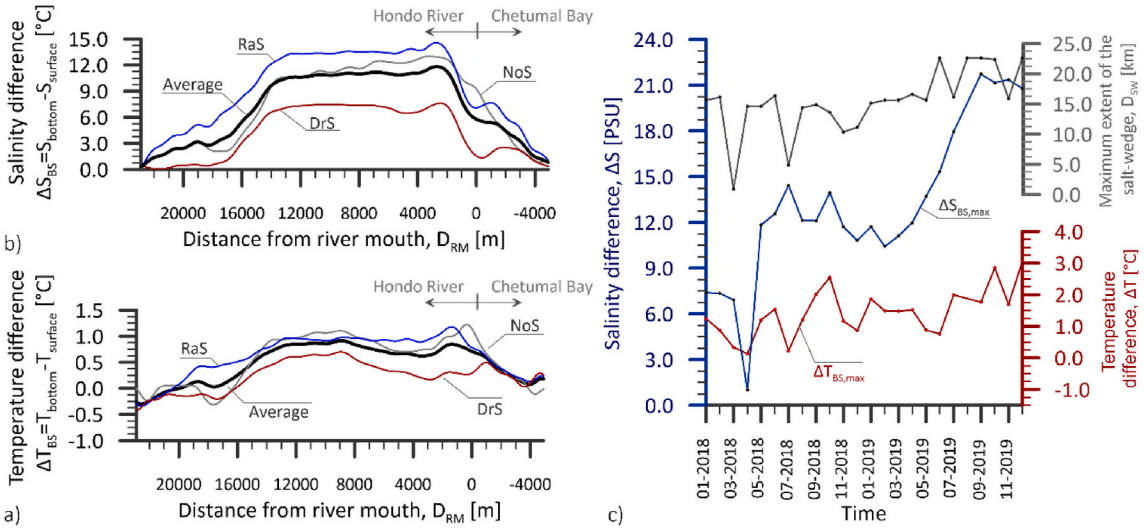

Fig. 3. Surface-to-bottom differences for a) temperature (ΔT_{BS}) and b) salinity (ΔS_{BS}) as a function of distance from the river mouth and of the season. Maximum differences per month for salinity and temperature along the riverine estuary and maximum extent of the salt-wedge are also shown (c).

St. 35 and the maximum extent of the salt-wedge, $D_{RM} = 22.6$ km.

The average water temperature profile is shown in Fig. 2c. The highest river temperatures ($T > 29.6$ °C) were present at $D_{RM} \approx 0$ km in the river mouth, corresponding to the location of reduced water depths ($d \sim 2.2$–4.0 m). From this point, surface water temperature decreased upstream of the Hondo River estuary and downstream toward Chetumal Bay. Additionally, temperature values observed underneath the pycnocline in the river estuary for $0.0 < D_{RM} < 16.2$ km were higher ($T > 29.4$ °C) than those observed at $D_{RM} < 0$ km toward Chetumal Bay ($T < 29.0$ °C). Similar to the salt-wedge development, the maximum extent of the thermocline occurred in September 2019, together with the maximum bottom-to-surface temperature difference $\Delta T_{BS,\,max} = 2.78$ °C (Fig. 3c).

Slight differences in the bottom-to-surface temperature existed between the RaS and NoS along the river estuary. Values ranging $\Delta T_{BS} = 0.8$–1.2 °C are described from the river mouth up to $D_{RM} = 14.1$ km, with variations of ΔT_{BS} decreasing continuously upstream (Fig. 3b). During the DrS, the values of ΔT_{BS} were approximately 65% smaller (i.e. $\Delta T_{BS} = 0.3$–0.7 °C) for $0.0 < D_{RM} < 14.1$ km. A negative ΔT_{BS} value indicated that the surface had a higher temperature than the bottom, as observed at $D_{RM} > 20.5$ km in the RaS and $D_{RM} > 16.3$ km in the NoS and DrS. These values are closely related to the extension of the salt-wedge (Figs. 2 and 3c). This distribution opposes the river estuary conditions, where the bottom-to-surface temperatures were exclusively positive. The peaks of ΔT_{BS} values were observed at the river mouth but mainly developed during the NoS and RaS. In the river delta and toward Chetumal Bay, the bottom-to-surface temperature difference decreased continuously throughout all seasons, reaching values of $\Delta T_{BS} \approx 0.2$ °C.

A decrease in salinity (approximately 0–2 PSU) occurred at the connection of the river estuary with the Chaac River, located in the final stretch of the salt-wedge. Temperature changes (<0.2 °C) due to the Chaac River influence were almost negligible. Additionally, the Four Miles Lagoon did not exhibit significant effects on the river estuary regarding either salinity or temperature.

3.2. Gibbs energy distribution in the Hondo River estuary

The T–S diagram as a function of the Gibbs energy (G_{HRE}) was drawn using Eq. (3) considering the water temperature and salinity at all profile points measured in the river estuary during 2018 and 2019 (Fig. 4). The minimum, mean, and maximum temperatures were $T_{min} = 23.76$ °C, $T_{mean} = 28.84$ °C, and $T_{max} = 33.44$ °C whereas for salinity they were $S_{min} = 5.45$ PSU, $S_{mean} = 23.76$ PSU, and $S_{max} = 25.26$ PSU.

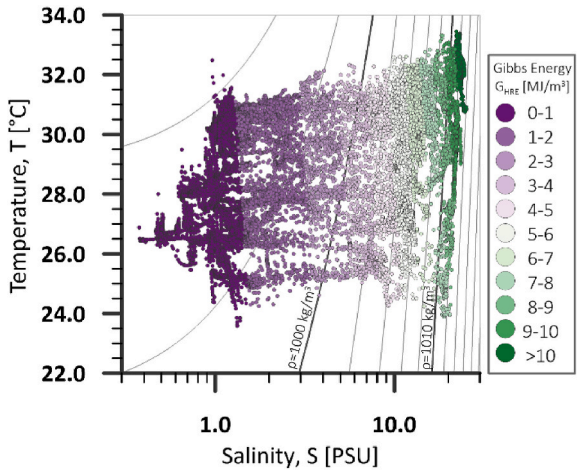

Fig. 4. T–S diagram as a function of the Gibbs energy considering the state (pressure, temperature, and ion concentration) of the water along the Hondo River estuary (G_{HRE}).

Approximately 61.6% of the water temperature and salinity conditions led to $0 < G_{HRE} < 2$ MJ/m^3, 19.4% to $2 < G_{HRE} < 6$ MJ/m^3, 17.0% to $6 < G_{HRE} < 10$ MJ/m^3, and 2.0% to $G_{HRE} > 10$ MJ/m^3.

In general, conditions with $6 < G_{HRE} < 10$ MJ/m^3 were found in almost all months in 2018 and 2019, with no clear dependency on the season. These conditions were observed for $S > 10.7$ PSU and a wider range of temperatures (i.e. $23.9 < T < 33.4$ °C) (Fig. 4). The river estuary water conditions leading to $G_{HRE} > 10$ MJ/m^3 occurred in all cases with $T > 29.0$ °C water temperature and $S > 20.14$ PSU salinities in 2019 during the RaS. Furthermore, the combinations of water temperature $T > 30.7$ °C and salinity $S > 22.8$ PSU were required to achieve $G_{HRE} > 10.5$ MJ/m^3, thereby indicating that an increase of the Gibbs energy depends on both temperature and salinity in the river estuary.

The Gibbs energy was estimated up to $G_{HRE} = 10.80$ MJ/m^3 and was related to a combination of high salinity ($S = 24.73$ PSU) and temperature ($T = 32.06$ °C) conditions. The location of the higher G_{HRE} values occurred upstream of the river mouth at $D_{RM} = 2.3$–2.8 km. This corresponds to the observed ΔS_{BS} and ΔT_{BS} peaks (Fig. 3) observed at a bathymetric depression in the river estuary (Fig. 2). Additionally, the maximum Gibbs energy occurred in September 2019, similar to the increase in the stratification and the extent of the salt-wedge.

Calculated G_{HRE} variations along the Hondo River estuary are described in Fig. 5 as a function of their relative frequency per kilometre (0.0–1.0). The Gibbs energy in the upper river estuary was $G_{HRE}<1$ MJ/m^3, with a relative frequency per kilometre of 0.70–0.90 for $14.0<D_{RM}<18.0$ km and more than 0.90 for $D_{RM}<21.0$ km. In the middle river estuary and up to the river mouth (i.e. $0.0<D_{RM}<14.0$ km), G_{HRE} values increased with a relative frequency per kilometre of approximately 0.60 for G_{HRE} = 0–3 MJ/m^3. In the river delta, the transition to higher G_{HRE} values reduced the relative frequency per kilometre of specific G_{HRE} intervals (i.e. the frequency was 0.67 for G_{HRE} = 1–5 MJ/m^3 at $D_{RM} = -1.0$ km, 0.74 for G_{HRE} = 4–8 MJ/m^3 at $D_{RM} = -3.0$ km, and 0.73 for G_{HRE} = 6–11 MJ/m^3 at $D_{RM} = -4.0$ km). Values exceeding $G_{HRE} = 10$ MJ/m^3 were commonly detected at St. 35 and St. 34 at Chetumal Bay with a relative frequency per kilometre greater than 0.19, which further decreased upstream of the river estuary, except at D_{RM} = 8.0–10.0 km, where the frequency reached values of 10.8–13.2%.

River discharge influenced the Gibbs energy transition at the delta and the salt intrusion upstream of the Hondo River estuary. The theoretical and environmental SGE potential are affected when accounting for the natural river discharge Q_N (Eq. (4) and Eq. (5)). The velocity profiles and depth-averaged velocities over the cross-section of the river mouth at St. 1 (Fig. 1) describe the incidence of positive and negative discharge events (Fig. 6). Positive river discharge events were commonly observed with downstream velocities ranging 0.1–0.3 m/s (Fig. 6a). Salt intrusion was usually lower than the river discharge, resulting in a positive net discharge ($Q_N > 0$). Contrastingly, negative river discharge events occurred when the salt intrusion upstream was higher than the downstream river discharge, leading to a negative net discharge ($Q_N < 0$). Water velocities decreased notably during negative river discharge events, presenting both positive (downstream) and negative (upstream) velocities (Fig. 6b).

The major influence of Chetumal Bay salt intrusion occurred over the left bank of the Hondo River on the Mexican side (Fig. 6). Moreover, a laterally sheared exchange flow was observed during the positive river discharge event in June 2018, with outflows on the right bank and inflows on the left bank. This flow configuration occurred in the river mouth and further developed in the salt-wedge formation (Fig. 2b) with a stronger vertical stratification (Fig. 3a). During negative river events, the river mouth was highly affected by salt inflow (Fig. 6b), primarily at a distance over the cross-section of $25<D_{CS}<55$ m and along the water column. The mixed conditions may reflect a decrease in the bottom-to-surface salinity difference along the river estuary (Fig. 3a).

Negative river discharge events were registered in June 2018 and April 2019 during the DrS. Positive discharge events occurred throughout the year but with an increase in magnitude during the NoS, when the influence of trade winds decreased. Despite negative river discharge events and increased salt intrusion during the DrS, the maximum salt-wedge extension and the bottom-to-surface salinity gradient occurred during the RaS. Hence, the seasonality of the thermohaline conditions reflects its variability in the Gibbs energy values, particularly at the river mouth, where a wider range of G_R values described a dispersed relative frequency (Fig. 5).

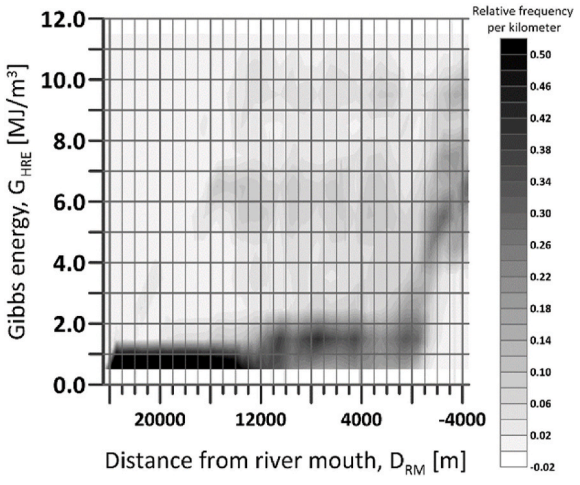

Fig. 5. Relative frequency of the calculated Gibbs energy (G_{HRE}) at each kilometre of the Hondo River estuary.

3.3. Theoretical and environmental SGE potential in the Hondo River estuary

The theoretical SGE potential in the Hondo River estuary was estimated (Eq. (5)), with the required water temperature, salinity, and river discharge conditions summarised in Table 1. An increase in the natural river discharge (Q_N) is related to an expected increase in TP, as observed at the end of the NoS in 2018 (Table 1 and Fig. 7). However, the trend changed owing to a combination of salinity values at Chetumal Bay and water river discharge. For example, higher salinities increased the theoretical SGE potential despite a decrease in river discharge, as observed in July 2019, when a higher S_{BaCh} of 21.3 PSU and a Q_N of 37.7 m^3/s led to higher TP values than months with a $Q_N > 40$ m^3/s but a $S_{BaCh}<17$ PSU. Similarly, S_{BaCh} of 21.7 PSU and Q_N of 19.44 m^3/s provided a TP of 15.25 MW, similar to that provided by an S_{BaCh} of 9.69 PSU and a higher Q_N of 53.77 m^3/s, thus leading to a comparable average theoretical SGE potential of TP = 15.24 MW. During the presence of negative discharge events, as presented in June 2018 and April 2019, TP was zero as Q_N was negative.

The temperature differences between the Hondo River estuary limits were up to 1.2 °C, 3–4 times lower than the vertical stratification and 5–21 times lower than the horizontal salinity gradient found in the estuary. Additionally, a minor influence of temperature on the estimation of TP was noticed despite the observed temporal variations in the range of 26.1–30.90 °C (Table 1). The average temperature at the Hondo River estuary limits was T = 28.6–28.8 °C; therefore, if an average temperature is considered (i.e. T = 28.7 °C) rather than the actual measured temperatures, the error in the TP estimation does not exceed the 2.1%. Therefore, the temporal variations in temperature in the Hondo River estuary might not be relevant for calculating the theoretical SGE potential.

The design and environmental flow were estimated to further define the CF and calculate EE. The mean river discharge during the measurement period was Q_{mean} = 35.92 m^3/s resulting in an environmental flow of $Q_E = 0.30 \bullet Q_{mean}$ = 10.78 m^3/s and a design flow of Q_D = EF•Q_{mean} = 7.18 m^3/s by considering the extraction factor EF = 0.20.

The operational conditions for an SGE plant can be determined based on the definitions of Q_E, Q_D, and natural river flow Q_N (Fig. 7 and Table 1). Full capacity operation periods (OPs) are generally defined for the Hondo River estuary, with limited zero operational periods (ZEP). ZEP occurred during negative discharge events when $Q_N < 0$ during the DrS of 2018 and 2019. Additionally, during the mid-summer drought in August 2018, further ZEP developed when $Q_N < Q_E$. A general decrease in the bottom-to-surface salinity and temperature during the ZEPs was also observed (Fig. 3c), indicating a general mixed condition of the estuary during these periods. The incidence of ZEPs is critical for designing the SGE plant and analysing the environmental effects of limited river discharge during these periods. Partial operation conditions (REP) might occur close to the ZEP when the residual river discharge Q_R equals or exceeds the Q_E but cannot supply the desired Q_D. The duration of the REPs during the year may vary, as shown in Fig. 7. The REP conditions found in 2019 were primarily related to the DrS when the Q_N was significantly reduced during the season. However, no REP conditions developed alongside the ZEP during the mid-summer drought in 2019 because Q_N was only reduced amid a generally increasing river discharge trend during the RaS.

The capacity factor was CF = 0.756, based on the expected Q_D and the monthly operational condition given by the Q_{OP} during the analysed

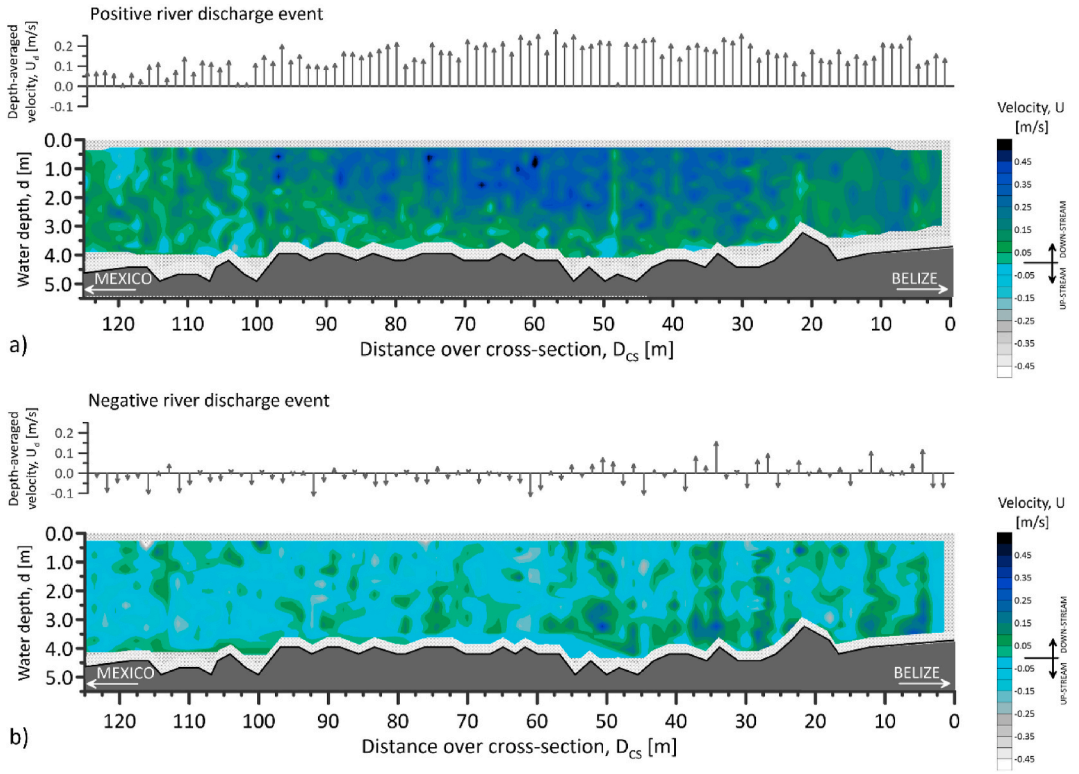

Fig. 6. Velocity profiles and depth-averaged velocities over the cross-section of the river mouth (St. 1) during a) positive river discharge event (December 2018) and b) negative river discharge event (June 2018), considering the effects of salt intrusion from Chetumal Bay.

Table 1
Estimated theoretical energy potential from salinity gradients based on the monthly variations of temperature, salinity, and water discharge. Operational and residual discharges are also provided, considering the operational condition.

Date	T_{RHo} [°C]	T_{BaCh} [°C]	S_{RHo} [PSU]	S_{BaCh} [PSU]	Q_N [m^3/s]	TP [MW]	Type of operation		Q_{OP} [m^3/s]	Q_R [m^3/s]
2018–02	26.12	27.36	0.93	9.69	53.77	15.24	OP	Full Capacity	7.18	46.59
2018–03	26.46	26.84	0.48	11.53	57.04	23.93	OP	Full Capacity	7.18	49.85
2018–04	28.33	28.19	0.88	14.29	–	–	–	–	–	–
2018–05	29.61	29.83	0.98	14.45	24.25	11.70	OP	Full Capacity	7.18	17.07
2018–06	30.36	29.53	0.98	14.68	−12.12	0.00	ZEP	No operation	0.00	−12.12
2018–07	29.98	29.95	0.99	17.25	43.71	26.13	OP	Full Capacity	7.18	36.53
2018–08	30.20	30.42	0.91	16.08	50.93	29.10	OP	Full Capacity	7.18	43.75
2018–09	30.04	30.68	0.96	16.02	5.492	3.10	ZEP	No operation	0.00	5.49
2018–10	29.24	29.23	0.88	16.13	60.47	33.88	OP	Full Capacity	7.18	53.29
2018–11	27.90	29.12	0.64	12.58	73.56	33.56	OP	Full Capacity	7.18	66.38
2018–12	27.45	28.24	0.91	13.20	90.75	38.94	OP	Full Capacity	7.18	83.57
2019–01	26.24	25.72	0.95	13.04	41.34	16.21	OP	Full Capacity	7.18	34.16
2019–02	26.60	26.82	0.92	13.41	16.85	7.09	REP	Partial operation	6.07	10.78
2019–03	27.48	27.46	1.00	15.12	–	–	–	–	–	–
2019–04	28.55	29.05	1.00	5.76	−0.95	0.00	ZEP	No operation	0.00	−0.95
2019–05	29.49	28.95	1.37	18.75	12.39	7.28	REP	Partial operation	1.61	10.78
2019–06	29.98	30.33	1.03	21.74	19.44	15.25	OP	Full Capacity	7.18	12.26
2019–07	30.50	30.90	1.05	21.30	37.75	29.15	OP	Full Capacity	7.18	30.57
Average	28.58	28.81	0.94	14.72	35.92					

*ZEP: zero extraction period; i.e. $Q_N < Q_E$. REP: reduced extraction period; i.e. $Q_E < Q_N < (Q_D + Q_E)$. OP: full operational period; i.e. $Q_N > (Q_D + Q_E)$.

period (Table 1). For a SGE plant installed under the conditions described in Table 1, the CF may represent a percentage within a year of the ideal operation of the SGE plant because of environmental and technical restrictions, such that the value of CF may imply a functioning at full capacity of approximately 6620 h/yr.

Thus, the annual practicable extractable energy was EE = 26,364 MWh/yr (Eq. (6)), corresponding to an approximately 3 MW SGE plant, for which the mean TP was 19.41 MJ/m^3 for an annual period between February 2018 and February 2019. Additionally, the annual environmental potential was up to EP = 34,874 MWh/yr by considering Eq. (7), where EP encompasses the potential of the estuarine system for SGE extraction by assuming a certain number of ZEPs could occur within a year. The EF was initially set to approximately 20% (i.e. 2.4 months with ZEP) as an approximation of the operational conditions and to estimate the EE and EP. This assumption was close to the actual ZEPs that occurred during the annual analysed period, with 2.0 months of DrS and mid-summer drought, resulting in a suitable and reliable constraint for continuous SGE harnessing.

According to Cerón-Palma et al. (2013), the electric energy consumption of low-income housing under similar tropical weather conditions was approximately 3.39 MWh/yr without an artificial cooling system but can increase to 6.46 MWh/yr with air conditioning. Notably,

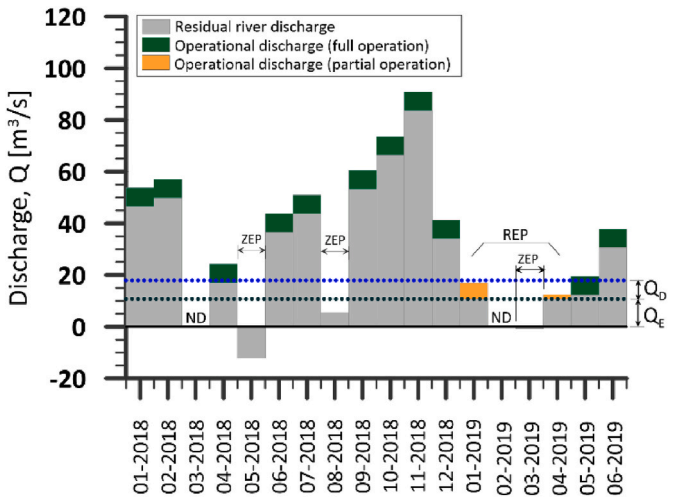

Fig. 7. Monthly Hondo River discharge records with the representation of possible full and partial operational conditions (Q_{OP}) considering the design flow (Q_D) and environmental discharge (Q_E). Conditions for reduced (REP) and zero extraction periods (ZEP) are also provided.

energy consumption was estimated to be up to 9.37 MWh/yr (Martínez-Sosa, 2019). From these estimations, the annual EE from the Hondo River estuary could be sufficient to supply electricity to approximately 7770 houses without a cooling system or approximately 2770–4050 houses with air conditioning and higher energy consumption. This represents an energy consumption of 5.4–15.1% of the houses in Chetumal, which accounts for approximately 51, 425 houses according to INEGI (2021).

The theoretical potential of the Hondo River estuary allows energy yield assessment for SGE harnessing for human consumption. However, comparing the estimated SGE potentials (TP, EE, and EP) with the percentage of manatee sightings within a year, based on Callejas-Jiménez et al. (2021), allowed the exploration of possible implications of SGE harnessing (Fig. 8). Higher EE and EP potentials occurred during the RaS, primarily between September and November, when manatee sightings decreased to a minimum. Moreover, the percentage of manatee sightings decreased considerably in the riverine estuary, while peaks in SGE potentials were present (e.g. February, June, and November). However, these SGE potential peaks were later followed by manatee sighting speaks, with a time lag of 1–2 months. Therefore, the residual potential after SGE extraction is still relevant, particularly during RaS

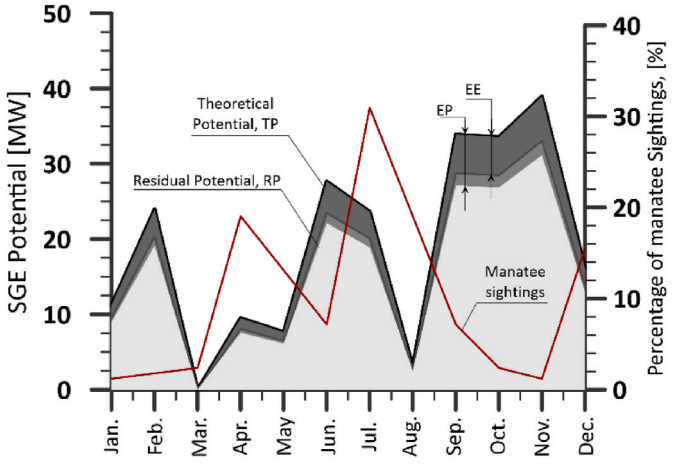

Fig. 8. Comparison of the SGE potential (TP, EE, and EP) in the riverine estuary environment and the estimated percentage of manatee presence based on reported sightings during 2018–2019 described in Callejas-Jiménez et al. (2021).

and the beginning of NoS, when the absolute magnitude of the TP is primarily harnessed, with higher values of EP and EE during an extended period preceding an increase in manatee sightings within a short period of the colder season of NoS.

4. Discussion and conclusions

This research examined the feasibility of a small estuarine system for SGE harnessing based on field dataset from multiannual monitoring. Small-scale generation schemes from renewable energies normally consider technologies for solar, wind, and biomass energies (Terrapon-Pfaff et al., 2014). However, marine renewables in the area form SGE showed the viability of a theoretical capacity of a SGE plant of ~3 MW, which could lead to an alternative cleaner production of energy, also broadening the viability of this type of renewable energy in further locations around the region. Seasonal and spatial longitudinal estuarine variations, ecological discharge, but also the presence of charismatic megafauna such as the manatee, resulted on the identification of a suitable scenario for SGE harnessing with estimated benefits for 7700 low-income houses for urban areas or commercial purposes in Mexico or Belize.

The seasonal changes in the thermohaline gradients of the Hondo River and site-specific constraints lead to the assessment of the environmental and technical SGE potential of the Mexico–Belize riverine estuary. SGE harnessing planning usually do not consider local spatio-temporal scales from river discharge as mentioned by Alvarez-Silva and Osorio (2015), which is usually accompanied by regular and episodic inputs of energy and material that affect the salt-wedge development (Day et al., 2019). Therefore, the conducted assessment of the thermohaline variations in the Hondo River represents a detailed basis for the SGE analysis.

During the RaS, a well-defined salt wedge with a larger extent (D_{RM}>16.3 km) and higher vertical stratification due to the increase in ΔS_{BS} and ΔT_{BS}-values (Fig. 3) was observed with the increase in freshwater flow and possible salt-intrusion enhancement from seasonal wind effects. Meanwhile, westerly wind events during the NoS and decreasing precipitation described a transition between the RaS and DrS. This transition is represented by a decrease in river discharge as well as the extent of the salt wedge and its vertical stratification (Table 1 and Fig. 3), which suggests that the riverine estuarine system is driven by a reduction in salt-intrusion effects from Chetumal Bay. The scenario changed to homogeneous or partially stratified conditions (i.e. maximum reduction of ΔS_{BS} and ΔT_{BS} values) with the development of shorter frontal areas during the DrS, notwithstanding the increase in easterly winds (Fig. 3). From the results, the Hondo River estuary can be recognised as a partially mixed estuary modulated by wind forcing effects, with a weak to moderate river discharge under a weak tidal condition. Therefore, the SGE potential at the Hondo River depends on the freshwater runoff of the river flowing to an extended mesohaline water body (Chetumal Bay), seasonally influenced by precipitation, trade winds, and cold fronts (Carrillo et al., 2009b).

The incidence of negative discharge events (i.e. higher inflow than outflow) in the DrS and amid the RaS by a mid-summer drought was driven by a significant decrease in the river flow (Table 1 and Fig. 6) and the possible salt-intrusion enhancement from easterly winds in the region (Yáñez-Arancibia and Day, 2004) that typically contrast with the orientation of the riverine estuary flow direction. These negative discharge events match with low SGE potentials and the development of ZEPs (Fig. 7). Since ZEPs could occur at periods of increased regional electricity demand, further analyses as described in Zachopoulos et al. (2022) should be developed. Besides the river discharge is inversely related to saltwater intrusion (Guerra-Chanis et al., 2019), the increase of river discharge allows a larger availability of freshwater to provide the difference of chemical potential between the diluted and concentrated solutions of NaCl in water (Emami et al., 2013). Nevertheless, further effects might affect the thermohaline structure in the Hondo

River estuary. Analyses of the transverse circulation, response on lateral flow and cross-sectional bathymetric effects on the thermohaline structure as in Valle-Levinson et al. (2000) and Yan et al. (2020) require further research for the Hondo River estuary as they might also be relevant for the SGE potential and for a better description of the estuarine hydrodynamics.

The freshwater discharge of the Hondo River is the dominant flow, confining the water supply of the Chaac and Ucum rivers, which have limited influence on time and space over the river estuarine conditions (Fig. 2). However, bathymetric structures close to the connections with the Chaac (D_{RM}≈16 km) and Ucum rivers (D_{RM}≈23 km) impact the extent of the salt wedge. In this regard, the average salt-wedge limit from the two-year measurements usually occurred at the mound at D_{RM}≈16 km, and its maximum recorded extent was constrained by the mound at D_{RM}≈23 km (Fig. 2). The river mound's effects on the salt-wedge extent were similar to those described by Alcérreca-Huerta et al. (2019) for a major tropical riverine estuary in the southern Gulf of Mexico. Similarly, the prominent bottom ridge at the Hondo River mouth influences the salinity variations along the riverine estuary as previously identified by Callejas-Jiménez et al. (2021).

The SGE potential resulting from the thermohaline structure of the Hondo River estuary is feasible for its harnessing under a local approach and site-specific constraints. The energy recovery of a hypothetical 3 MW SGE plant could be greater than 80% if considering reverse electrodialysis (RED) (Post et al., 2008) and up to 91.1% for pressure retarded osmosis (PRO) systems (Yip and Elimelech, 2012), but assuming zero losses from system components (Alvarez-Silva and Osorio, 2015).

SGE extraction is suitable for large rivers, as described by Alvarez-Silva et al. (2016), and simultaneously over a smaller local scale as identified by this research, thereby increasing the use of the SGE potential with a social benefit for the inhabitants. The Hondo River represents a case where thermohaline conditions of the estuarine environment allow local SGE harvesting. Thus, SGE could enhance energy security in the study area through a small-scale decentralized energy solution, for which continuous *in-situ* field measurements and monitoring of site-specific estuarine features are further required. These energy systems could increase the SGE potential as a renewable energy source (Zachopoulos et al., 2022).

The SGE plant capacity for the Hondo River is similar to hypothetical pilot plants described to approach the thermohaline structure of coastal lagoons or riverine estuaries in the Yucatan Peninsula with prototypes of 50 kW (Marin-Coria et al., 2021), 5.5 MW (Wojtarowski et al., 2021), and 3–24 MW (Martínez-Sosa, 2019). The EE in the scarce river estuaries of the Yucatan Peninsula, such as the Hondo River, provides the advantage of continuous water discharge (i.e. Q_D) for the mixing process with reduced ZEP and REP periods throughout the year, in contrast to coastal lagoons restricted by water sources. Additionally, the SGE potential may be increased by introducing alternative benefits, such as using treated wastewater from urban areas (Zoungrana et al., 2020). In this regard, the population settlements of Chetumal and Bacalar in the study area could increase the freshwater availability (~0.6 m^3/s) for SGE harnessing.

Changes in physicochemical factors, such as salinity, can trigger modifications in the structure and functionality of habitats and associated species (Licursi et al., 2010). Organisms including marine mammals (Corona-Figueroa et al., 2021), fishes (Lehmann et al., 2021), bivalves (McKeon et al., 2015), and plankton (Licursi et al., 2010) are sensitive to environmental variations. Potential negative environmental impacts from SGE harnessing relate to noise, land modification, and release of pollutants (Seyfried et al., 2019). Location of freshwater and brackish water intake points and disposal after mixing is highly relevant to avoid changes in the natural river mixing zone and the water quality for environmental sustainability. In this regard, the Hondo River estuary is considered an important Caribbean refuge for manatees (Callejas-Jiménez et al., 2021) and temporary or permanent loss of habitat and abandonment, stress, and physiological damage are recognised as possible negative effects of extracting SGE in the area. Thus, research should focus on a more detailed analysis of the estuarine hydrodynamics, its connectivity with further water bodies, impacts from punctual intake and output flows, and the environmental resilience before implementing a SGE plant.

Technical feasibility for SGE harnessing has been described for the Hondo River estuary. Nevertheless, a decrease in the estimated SGE potential (>50 kJ/m^3) owing to water transport, pre-treatment methods, membrane fouling, and conducts blockage should also be considered (Ju et al., 2022). Recent techno-economic analyses show that the levelized cost of energy for SGE ranges from 0.06 to 6.80 USD/kWh, being, in certain cases, cost-competitive among renewable energies but still dependent on site-specific conditions (Yip et al., 2016), the state's existing price of electricity, or the desired payback period (Naghiloo et al., 2015). Therefore, an economic assessment for SGE implementation in the Hondo River estuary should be further assessed, considering the needs and benefits within a binational framework between Mexico and Belize.

The SGE in the Hondo River exhibits a potential small-scale solution with an acceptable efficiency. Sustainable bilateral frameworks could be intended by encompassing partial energy coverage for low-income urban areas or a shared commercial approach in free zones. SGE harnessing depends on water pre-treatment methods to mitigate fouling or damage to membranes in RED (Ju et al., 2022) or PRO processes (Han et al., 2016). Hence, the water treatment required for SGE could, in parallel, boost environmental conservation owing to an improved water quality disposal in urban contexts (Cipollina et al., 2018), enhancing the benefits of SGE plant through a more suitable cost-effective scheme (Zoungrana et al., 2020).

Finally, feasible schemes for implementing renewable energies, such as SGE, should be explored in the area to encourage functional, regional, and sustainable development based on the site-specific conditions and a further understanding of the river estuarine hydrodynamics. Strategies, benefits, and limits for SGE systems should also be recognised to address local financial, economic, urban, and social demands while overcoming up-scaling SGE barriers (Ripken, 2015).

Declaration of competing interest

The authors declare that they have no known competing financial interests or personal relationships that could have appeared to influence the work reported in this paper.

Data availability

Data will be made available on request.

Acknowledgments

Funding for fieldwork expenses during the monthly field surveys is acknowledged to the first author. The APC funding is due to the first and second authors. The support is gratefully acknowledged to the COBIA Team for their navigation services and Lic. J.M. Rusconi for access to 'Villas Manatí' facilities in Chetumal, Mexico. The assistance of Martha Huerta-Sánchez in graphics development is also acknowledged. Recognition is given to the CONACYT (National Council for Science and Technology of Mexico) program 'Investigadoras e Investigadores por México' (Project 761).

Appendix A. Supplementary data

Supplementary data to this article can be found online at https://doi.org/10.1016/j.clet.2022.100562.

References

Alcérreca-Huerta, J.C., Callejas-Jiménez, M.E., Carrillo, L., Castillo, M.M., 2019. Dam implications on salt-water intrusion and land use within a tropical estuarine environment of the Gulf of Mexico. Sci. Total Environ. 652, 1102–1112. https://doi.org/10.1016/j.scitotenv.2018.10.288.

Alvarez-Silva, O., Osorio, A.F., 2015. Salinity gradient energy potential in Colombia considering site specific constraints. Renew. Energy 74, 737–748. https://doi.org/10.1016/j.renene.2014.08.074.

Alvarez-Silva, O., Winter, C., Osorio, A.F., 2014. Salinity gradient energy at river mouths. Environ. Sci. Technol. Lett. 1, 410–415. https://doi.org/10.1021/ez500239n.

Alvarez-Silva, O.A., Osorio, A.F., Winter, C., 2016. Practical global salinity gradient energy potential. Renew. Sustain. Energy Rev. 60, 1387–1395. https://doi.org/10.1016/j.rser.2016.03.021.

Budde, J., 2021. A comparison of reverse electrodialysis and pressure retarded osmosis as technologies for salinity gradient power. EGU Master J. Renew. Energy Short Rev. 72–78. https://doi.org/10.25974/ren_rev_2021_14.

Burton, J., Hubacek, K., 2007. Is small beautiful? A multicriteria assessment of small-scale energy technology applications in local governments. Energy Pol. 35, 6402–6412. https://doi.org/10.1016/j.enpol.2007.08.002.

Callejas-Jiménez, M.E., Alcérreca-Huerta, J.C., Morales-Vela, B., Carrillo, L., 2021. Spatial and seasonal variations in surface water temperature and salinity in the Mexico-Belize riverine estuary: possible comfort conditions for manatees? Mar. Mamm. Sci. 37, 1454–1474. https://doi.org/10.1111/mms.12838.

Carrillo, L., Palacios-Hernández, E., Ramírez, A.M., Morales-Vela, B., 2009a. Características hidrometeorológicas y batimétricas. In: Espinoza-Ávalos, J., Islebe, G. A., Hernández-Arana, H.A. (Eds.), El Sistema Ecológico de La Bahía de Chetumal/Corozal: Costa Occidental Del Mar Caribe. El Colegio de la Frontera Sur (ECOSUR), Chetumal, Mexico, pp. 12–20.

Carrillo, L., Palacios-Hernández, E., Yescas, M., Ramírez-Manguilar, A.M., 2009b. Spatial and seasonal patterns of salinity in a large and shallow tropical estuary of the western caribbean. Estuar. Coast 32, 906–916. https://doi.org/10.1007/s12237-009-9196-2.

CBB, 2019. 2019 Annual Report & Statement of Accounts for the Year Ending. Belize City, Belize.

Cerón-Palma, I., Sanyé-Mengual, E., Oliver-Solà, J., Montero, J.-I., Ponce-Caballero, C., Rieradevall, J., 2013. Towards a green sustainable strategy for social neighbourhoods in Latin America: case from social housing in Merida, Yucatan, Mexico. Habitat Int. 38, 47–56. https://doi.org/10.1016/j.habitatint.2012.09.008.

Cipollina, A., Di Silvestre, M.L., Giacalone, F., Micale, G.M., Riva Sanseverino, E., Sangiorgio, R., Tran, Q.T., Vaccaro, V., Zizzo, G., 2018. A methodology for assessing the impact of salinity gradient power generation in urban contexts. Sustain. Cities Soc. 38, 158–173. https://doi.org/10.1016/j.scs.2017.12.037.

Corona-Figueroa, M.F., Ríos, N., Castelblanco-Martínez, D.N., Vilchez-Mendoza, S., Delgado-Rodríguez, D., Niño-Torres, C.A., 2021. Searching for manatees in the dark waters of a transboundary river between Mexico and Belize: a predictive distribution model. Aquat. Ecol. 55, 59–74. https://doi.org/10.1007/s10452-020-09810-9.

Corrales-Suastegui, A., Fuentes-Franco, R., Pavia, E.G., 2020. The mid-summer drought over Mexico and Central America in the 21st century. Int. J. Climatol. 40, 1703–1715. https://doi.org/10.1002/joc.6296.

Day, J.W., Ramachandran, R., Giosan, L., Syvitski, J., Paul Kemp, G., 2019. Delta winners and losers in the anthropocene. In: Coasts and Estuaries. Elsevier, pp. 149–165. https://doi.org/10.1016/B978-0-12-814003-1.00009-5.

Deshmukh, R., Carvallo, J.P., Gambhir, A., 2013. Sustainable Development of Renewable Energy Mini-Grids for Energy Access: A Framework for Policy Design. Lawrence Berkeley National Laboratory, University of California, California, USA.

Emami, Y., Mehrangiz, S., Etemadi, A., Mostafazadeh, A., Darvishi, S., 2013. A brief review about salinity gradient energy. Int. J. Smart Grid Clean Energy 2, 295–300. https://doi.org/10.12720/sgce.2.2.295-300.

Emdadi, A., Gikas, P., Farazaki, M., Emami, Y., 2016. Salinity gradient energy potential at the hypersaline Urmia Lake – ZarrinehRud River system in Iran. Renew. Energy 86, 154–162. https://doi.org/10.1016/j.renene.2015.08.015.

Guerra-Chanis, G.E., Reyes-Merlo, M.Á., Díez-Minguito, M., Valle-Levinson, A., 2019. Saltwater intrusion in a subtropical estuary. Estuar. Coast Shelf Sci. 217, 28–36. https://doi.org/10.1016/j.ecss.2018.10.016.

Haddout, S., Priya, K.L., 2020. Impacts of flushing time and intrusion length on electricity production from salinity gradient energy (SGE) in the estuaries. Int. J. River Basin Manag. 1–3. https://doi.org/10.1080/15715124.2020.1750422.

Han, G., Zhou, J., Wan, C., Yang, T., Chung, T.-S., 2016. Investigations of inorganic and organic fouling behaviors, antifouling, and cleaning strategies for pressure retarded osmosis (PRO) membrane using seawater desalination brine and wastewater. Water Res. 103, 264–275. https://doi.org/10.1016/j.watres.2016.07.040.

Helfer, F., Sahin, O., Lemckert, C., Anissimov, Y., 2013. Salinity gradient energy: a new source of renewable energy in Australia. Water Util. J. 5, 3–13.

INEGI, 2022. Mapas. Cartas Topográficas 1:50,000 E16A66, E16A65, E16A75 [WWW Document]. URL. https://www.inegi.org.mx/app/mapas/.

INEGI, 2021. Principales resultados por localidad (ITER). Censo de Población y Vivienda 2020 [WWW Document]. URL. https://www.inegi.org.mx/programas/ccpv/2020/#Microdatos.

Ju, J., Choi, Y., Lee, S., Park, C., Hwang, T., Jung, N., 2022. Comparison of pretreatment methods for salinity gradient power generation using reverse electrodialysis (RED) systems. Membranes 12, 372. https://doi.org/10.3390/membranes12040372.

Kauffer, E., 2021. Hidroextractivismo en la cuenca del Usumacinta: entre dinámicas transfronterizas y diferenciaciones fronterizas/Hydroextractivism in the Usumacinta river basin: among transboundary dynamics and border differentation. Rev. Trace 171. https://doi.org/10.22134/trace.80.2021.792.

Kempener, R., Neumann, F., 2014. Salinity gradient energy. Tech. Brief (Brief 2, 28.

Khodadadian Elikaiy, S., Lari, K., Torabi Azad, M., Sabetahd Jahromi, A., Mohseni Arasteh, A., 2021. Investigation and evaluation of salinity gradient power in Arvand River estuary using pressure retarded osmosis (PRO) method. Int. J. Environ. Sci. Technol. 18, 463–470. https://doi.org/10.1007/s13762-020-02993-6.

Lehmann, A., Myrberg, K., Post, P., Chubarenko, I., Dailidiene, I., Hinrichsen, H.-H., Hüssy, K., Liblik, T., Lips, U., Meier, H.E.M., Bukanova, T., 2021. Salinity dynamics of the baltic sea. Earth Syst. Dyn. https://doi.org/10.5194/esd-2021-15.

Licursi, M., Gómez, N., Donadelli, J., 2010. Ecological optima and tolerances of coastal benthic diatoms in the freshwater-mixohaline zone of the Río de la Plata estuary. Mar. Ecol. Prog. Ser. 418, 105–117. https://doi.org/10.3354/meps08865.

Marin-Coria, E., Silva, R., Enriquez, C., Martínez, M.L., Mendoza, E., 2021. Environmental assessment of the impacts and benefits of a salinity gradient energy pilot plant. Energies 14, 3252. https://doi.org/10.3390/en14113252.

Martínez-Sosa, I., 2019. Evaluación del potential energético asociado a gradiente salino del Río Champotón. Universidad Autónoma de Campeche.

McKeon, C.S., Tunberg, B.G., Johnston, C.A., Barshis, D.J., 2015. Ecological drivers and habitat associations of estuarine bivalves. PeerJ 3, e1348. https://doi.org/10.7717/peerj.1348.

Meerman, J., Clabaugh, J., 2017. Biodiversity and environmental resource data system of Belize [WWW Document]. URL. http://www.biodiversity.bz/.

Mueller, K.E., Thomas, J.T., Johnson, J.X., DeCarolis, J.F., Call, D.F., 2021. Life cycle assessment of salinity gradient energy recovery using reverse electrodialysis. J. Ind. Ecol. 25, 1194–1206. https://doi.org/10.1111/jiec.13082.

Naghiloo, A., Abbaspour, M., Mohammadi-Ivatloo, B., Bakhtari, K., 2015. Modeling and design of a 25 MW osmotic power plant (PRO) on Bahmanshir River of Iran. Renew. Energy 78, 51–59. https://doi.org/10.1016/j.renene.2014.12.067.

Pachauri, S., Brew-Hammond, A., Barnes, D.F., Bouille, D.H., Gitonga, S., Modi, V., Prasad, G., Rath, A., Zerriffi, H., Dafrallah, T., Heruela, C., Kemausuor, F., Kowsari, R., Nagai, Y., Rijal, K., Takada, M., Wamukonya, N., 2012. Energy access for development. In: Team- GEA Writing (Ed.), Global Energy Assessment: toward a Sustainable Future. Cambridge University Press and IIASA, UK, pp. 1401–1458.

Popelka, S.J., Smith, L.C., 2020. Rivers as political borders: a new subnational geospatial dataset. Water Pol. 22, 293–312. https://doi.org/10.2166/wp.2020.041.

Post, J.W., Hamelers, H.V.M., Buisman, C.J.N., 2008. Energy recovery from controlled mixing salt and fresh water with a reverse electrodialysis system. Environ. Sci. Technol. 42, 5785–5790. https://doi.org/10.1021/es8004317.

Ripken, M., 2015. Blue Energy - Barriers of Up-Scaling Salinity Gradient Power. University of Groningen.

Roldan-Carvajal, M., Vallejo-Castaño, S., Álvarez-Silva, O., Bernal-García, S., Arango-Aramburo, S., Sánchez-Sáenz, C.I., Osorio, A.F., 2021. Salinity gradient power by reverse electrodialysis: a multidisciplinary assessment in the Colombian context. Desalination 503, 114933. https://doi.org/10.1016/j.desal.2021.114933.

Schaetzle, O., Buisman, C.J.N., 2015. Salinity gradient energy: current state and new trends. Engineering 1, 164–166. https://doi.org/10.15302/J-ENG-2015046.

Seyfried, C., Palko, H., Dubbs, L., 2019. Potential local environmental impacts of salinity gradient energy: a review. Renew. Sustain. Energy Rev. 102, 111–120. https://doi.org/10.1016/j.rser.2018.12.003.

Tedesco, M., Cipollina, A., Tamburini, A., Micale, G., 2017. Towards 1 kW power production in a reverse electrodialysis pilot plant with saline waters and concentrated brines. J. Membr. Sci. 522, 226–236. https://doi.org/10.1016/j.memsci.2016.09.015.

Terrapon-Pfaff, J., Dienst, C., König, J., Ortiz, W., 2014. A cross-sectional review: impacts and sustainability of small-scale renewable energy projects in developing countries. Renew. Sustain. Energy Rev. 40, 1–10. https://doi.org/10.1016/j.rser.2014.07.161.

Valle-Levinson, A., Li, C., Wong, K.-C., Lwiza, K.M.M., 2000. Convergence of lateral flow along a coastal plain estuary. J. Geophys. Res. Ocean. 105, 17045–17061. https://doi.org/10.1029/2000JC900025.

Vallejo-Castaño, S., Sánchez-Sáenz, C.I., 2017. Design and optimization of a reverse electrodialysis stack for energy generation through salinity gradients. DYNA 84, 84–91. https://doi.org/10.15446/dyna.v84n202.59321.

Vivid Economics, 2019. Regional Economic Development: Master Plan for Corozal District, Belize. London, UK.

Wojtarowski, A., Martínez, M.L., Silva, R., Vázquez, G., Enriquez, C., López-Portillo, J., García-Franco, J.G., MacGregor-Fors, I., Lara-Domínguez, A.L., Lithgow, D., 2021. Renewable energy production in a Mexican biosphere reserve: assessing the potential using a multidisciplinary approach. Sci. Total Environ. 776, 145823 https://doi.org/10.1016/j.scitotenv.2021.145823.

Yan, Y., Song, D., Bao, X., Ding, Y., 2020. The response of lateral flow to peak river discharge in a macrotidal estuary. Water 12, 3571. https://doi.org/10.3390/w12123571.

Yáñez-Arancibia, A., Day, J.W., 2004. Environmental sub-regions in the Gulf of Mexico coastal zone: the ecosystem approach as an integrated management tool. Ocean Coast Manag. 47, 727–757. https://doi.org/10.1016/j.ocecoaman.2004.12.010.

Yip, N.Y., Brogioli, D., Hamelers, H.V.M., Nijmeijer, K., 2016. Salinity gradients for sustainable energy: primer, progress, and prospects. Environ. Sci. Technol. 50, 12072–12094. https://doi.org/10.1021/acs.est.6b03448.

Yip, N.Y., Elimelech, M., 2012. Thermodynamic and energy efficiency analysis of power generation from natural salinity gradients by pressure retarded osmosis. Environ. Sci. Technol. 46, 5230–5239. https://doi.org/10.1021/es300060m.

Zachopoulos, K., Kokkos, N., Elmasides, C., Sylaios, G., 2022. Coupling hydrodynamic and energy production models for salinity gradient energy assessment in a salt-wedge estuary (strymon river, northern Greece). Energies 15, 2970. https://doi.org/10.3390/en15092970.

Zoungrana, A., Türk, O.K., Çakmakci, M., 2020. Energy coverage of ataköy-ambarlı municipal wastewater treatment plants by salinity gradient power. J. Water Proc. Eng. 38, 101552 https://doi.org/10.1016/j.jwpe.2020.101552.